Free surface stability of liquid metal plasma facing components

IOP Publishing | International Atomic Energy Agency Nuclear Fusion

Nucl. Fusion **56** (2016) 106020 (10pp) doi:10.1088/0029-5515/56/10/106020

Free surface stability of liquid metal plasma facing components

P. Fiflis, M. Christenson, M. Szott, K. Kalathiparambil and D.N. Ruzic

Department of Nuclear, Plasma and Radiological Engineering, Center for Plasma Material Interactions, University Illinois at Urbana-Champaign, Urbana, IL 61801, USA

E-mail: fiflis1@illinois.edu

Received 28 April 2016, revised 13 July 2016
Accepted for publication 18 July 2016
Published 16 August 2016

Abstract

An outstanding concern raised over the implementation of liquid metal plasma facing components in fusion reactors is the potential for ejection of liquid metal into the fusion plasma. The influences of Rayleigh–Taylor-like and Kelvin–Helmholtz-like instabilities were experimentally observed and quantified on the thermoelectric-driven liquid-metal plasma-facing structures (TELS) chamber at the University of Illinois at Urbana–Champaign. To probe the stability boundary, plasma currents and velocities were first characterized with a flush probe array. Subsequent observations of lithium ejection under exposure in the TELS chamber exhibited a departure from previous theory based on linear perturbation analysis. The stability boundary is mapped experimentally over the range of plasma impulses of which TELS is capable to deliver, and a new theory based on a modified set of the shallow water equations is presented which accurately predicts the stability of the lithium surface under plasma exposure.

Keywords: lithium, plasma facing component, stability

(Some figures may appear in colour only in the online journal)

1. Introduction

Liquid lithium has gathered growing interest within the fusion community in recent years as a divertor, limiter, and alternative first wall material. Liquid lithium is attractive as a low-Z material replacement for refractory metals due to its ability to getter impurities, while also being self-healing in nature. However, concerns exist about the stability of a liquid metal surface at the edge of a fusion device. One of the first experiments to employ macroscopic quantities of liquid lithium was the D-IIID tokamak with the utilization of a lithium target on the divertor material evaluation system (DiMES) probe. Initial concerns about lithium revolved around enhanced erosion of a liquid in a fusion environment as opposed to a solid as well as the fluid stability under the presence of strong currents and magnetic fields. Exposures with solid lithium showed no issue, however, even during quiescent exposures, the liquid lithium was sufficiently perturbed by plasma forces to eject small droplets of lithium into the plasma. Radial sloshing of the lithium pool was explained as movement due to $J_z \times B$ forces, and vertical injection into the core plasma is thought to be due to radial currents flowing through the lithium and interacting with the main toroidal field [1].

An additional explanation however, may be offered by the exposure of a liquid melt layer to strong plasma flows [2]. Experiments performed in the quasi-stationary plasma accelerator (QSPA-T) suggest that ejection of tungsten droplets from a thin melt layer due to plasma exposure is a result of the growth of Kelvin–Helmholtz instabilities growing on the surface of the tungsten. Droplet formation in this case is attributed to frictional forces on the tungsten melt from the plasma (Kelvin–Helmholtz instabilities). Finally, a study of melted tungsten lamellae from the 2009 campaign of Alcator C-Mod suggests that the movement of the melted tungsten was consistent with a combination of $J \times B$ and plasma pressure forces [3].

A liquid lithium limiter was employed on the current drive experiment upgrade (CDX-U) at Princeton Plasma Physics Laboratory. In stark contrast to the experiments of the Li-DiMES probe, the lithium tray used in CDX-U showed a lack of mechanical motion due to $J \times B$ forces [4], even though the currents present in the lithium (typical 200–300 kA m^{-2},

for short times in excess of 1 MA m^{-2}) were still very large. This is explained by the CDX-U design forcing all ground currents flowing through the lithium to flow toroidally (aligned with the magnetic field) rather than perpendicular to the field. The only ejection observed over the course of hundreds of discharges was that of a small amount of lithium due to the formation of unipolar arcs early in the first campaign. The arcs were thought to be to large impurities present on the lithium surface. As a result of the success of the CDX-U experiments, the National Spherical Tokamak Experiment (NSTX) installed and began operation of a liquid lithium divertor. Macroscopic ejection of lithium has also not been observed in the NSTX LLD, although the NSTX LLD is not very deep.

A proposed alternative concept for a liquid metal divertor has been demonstrated with the lithium metal infused trenches (LiMIT) experiments performed at UIUC and elsewhere [5–7]. LiMIT uses thermoelectric magnetohydrodynamic (TEMHD) flow [5] to self-propel lithium down a series of trenches, employing lithium as both a plasma facing surface and a coolant. TEMHD flow relies on a thermal gradient to drive thermoelectric currents that then interact with a magnetic field to drive flow; in the case of a tokamak this magnetic field would be the main toroidal field.

Initial observations of lithium ejection at the University of Illinois were observed during a series of tests where the LiMIT trenches were placed into the thermoelectric liquid-metal plasma facing structures (TELS) chamber and fired upon. A fast frame camera observed the shots to record instances of ejection. Fast frame videos of the shots were taken and reduced to the few frames following plasma impact where droplets of lithium can be seen exiting the LiMIT trenches. Initial observations indicate an overfill of lithium at the bottom of the tray was the location of the lithium ejection. No lithium was observed to exit the channels, consistent with the hypothesis that the lithium channels act to stabilize instability growth on the surface. Lithium ejection from the pool was large, and fast frame camera diagnosis shows formation of a complex structure on top of the lithium which appears to break up due to surface tension forces. Initial attempts to alleviate ejection of lithium involved placing a thin mesh over the lower lithium pool to attempt to retain the lithium. However, lithium wicked through the mesh, forming a pool regardless, which then continued to eject lithium. Pooling of the same degree was not observed during tests performed with the LiMIT structures on the Magnum PSI device [7], even though more extreme angles of exposure were employed. This may be attributable to the presence of side trenches in the design employed within TELS. Lithium in the Magnum design was retained against gravity by surface tension in the trenches. The presence of a large side channel in the TELS design was not able to exert the same surface tension forces, allowing the lithium to flow with gravity and form a pool at the bottom of the structure. It can be seen from the experiments discussed thus far that a stability boundary exists between large pools of liquid metal and constrained liquid metal surfaces. As this stability boundary was previously not mapped experimentally, an in-depth examination is presented here.

2. Analytic Rayleigh–Taylor/Kelvin–Helmholtz stability boundary

An analysis of the $J \times B$ forces on the lithium in the NSTX LLD was performed by Jaworski *et al* [8]. The stability analysis performed suggests stabilization of the $J \times B$ driven Rayleigh–Taylor instabilities by surface tension of the lithium. In order to gain an understanding of the relative importance of various forces on a free liquid lithium surface, the Rayleigh–Taylor analysis performed by Jaworski *et al* [8] was expanded to include Kelvin–Helmholtz instabilities. When reduced to a dispersion relation, the result of this analysis is given by:

$$\omega = vk \pm \mathrm{i}\sqrt{\frac{\rho_{\mathrm{Li}} - \rho_{\mathrm{plas}}}{\rho_{\mathrm{Li}} + \rho_{\mathrm{plas}}} kg\cos(\theta) + \frac{f_{\mathrm{Li}}}{\rho_{\mathrm{Li}} + \rho_{\mathrm{plas}}} k - \frac{\gamma k^3}{\rho_{\mathrm{Li}} + \rho_{\mathrm{plas}}} + \frac{\rho_{\mathrm{Li}}\rho_{\mathrm{plas}}}{(\rho_{\mathrm{Li}} + \rho_{\mathrm{plas}})^2}(v_{\mathrm{Li}} - v_{\mathrm{plas}})^2 k^2} = 0 \quad (1)$$

Where ω is the frequency, k the wavenumber, v the velocity, ρ the mass density, g acceleration due to gravity, f the magnitude of a body force, and γ surface tension of the lithium. The imaginary portion of the frequency corresponds to the growth rate of the instability. For $\mathrm{Im}(\omega) > 0$, the wave is unstable, for $\mathrm{Im}(\omega) < 0$, the wave is stable.

The terms under the root are, in order, gravity, other body forces acting on the lithium (such as $J \times B$ forces), stabilization of the interface due to surface tension, and destabilization of the surface due to Kelvin–Helmholtz instabilities. The first two terms may be classified as Rayleigh–Taylor (RT) like instabilities, while the final term is Kelvin–Helmholtz (KH) like. Stabilization is accomplished via surface tension. A graph of the imaginary portion of the frequency versus the wavenumber is shown in figure 1 for a variety of mass flows of plasma across a static lithium surface that is being exposed to $J \times B$ forces.

It can be seen that as wavenumber increases, because of the cubic dependence on wavenumber, a lithium surface will always be stable to RT and KH instabilities. The wavenumber above which a lithium surface is stable is alluded to by Jaworski *et al* [8] as the critical wavenumber for a given set of conditions e.g. temperature, current, magnetic field. Because a liquid feature of a given dimension only permits wavenumbers above a certain value, the critical wavenumber may then be converted to a maximum lithium feature dimension that will not eject droplets due to RT and KH instabilities. Hereforth, reference will only be made to the maximum feature dimension which corresponds to the minimum stable wavenumber.

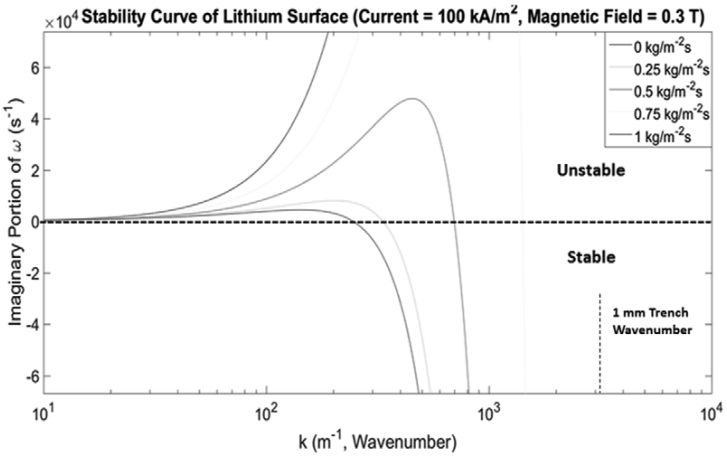

Figure 1. Stability curve for a liquid lithium free surface exposed to destabilizing $J \times B$ forces, stabilizing gravity forces, and flow of plasma across the surface engendering Kelvin–Helmholtz instabilities. It can be seen that for different impinging plasma velocities that the stability for intermediate wavenumbers is dominated by Kelvin–Helmholtz instabilities, however, these are stabilized by restriction to high wavenumber with the use of small lithium channels. Mass flux for several of the theta shots was approximately 0.5 kg m^{-2} s^{-1}.

3. Characterization of RT and KH Drivers in the TELS test stand

To test the derived stability boundary for liquid metal plasma facing components, a series of tests were performed in the TELS test stand at the University of Illinois. TELS is equipped with a coaxial plasma gun which is then pinched with a theta pinch, greatly increasing the temperature of the plasma at the expense of a small decrease in density. The theta pinch is fed by a large capacitor bank (36 μF, maximum voltage 60 kV). Diagnosis with calorimetry has shown energy densities of 0.15 MJ m^{-2} deposition on target (roughly equivalent to an ASDEX Type I ELM [9]) in approximately 150 μs. Characterization of the plasma with triple Langmuir probes and RFEAs has yielded an ion temperature of approximately 20 eV after use of the theta pinch [10], and use of photodiodes has shown an approximate plasma velocity of 65 km s^{-1} [11]. Subsequently, a fast frame camera (Vision Research Phantom Miro eX4 Color Camera) is used to characterize lithium ejection during shots. Characterization of the TELS device was performed while varying the voltage on the coaxial plasma gun with and without the firing the theta pinch.

TELS was diagnosed to capture the relevant parameters for droplet ejection from the lithium. TELS was diagnosed under four different experimental conditions: two with only the coaxial gun at 5.5 kV and 6 kV, and two with both the coaxial gun and the theta pinch at 5.5 and 6 kV on the coaxial gun and 16 kV on the theta pinch. Destabilization due to Rayleigh–Taylor instabilities via $J \times B$ forces on the lithium were quantified by means of a series of flush-mounted current probes assembled into a circular flush probe array (CFPA), similar in concept to the High Density Langmuir Probe Array on NSTX [12]. The magnetic field strength inside TELS is set by external magnets ($B_{max} = 0.22$ T). Currents in the TELS plasma were measured with the flush probe array. A photo of the array can be seen in figure 2. Axial, radial, and azumithal currents were measured via connecting the probe heads to each other and to ground in different configurations. By connecting

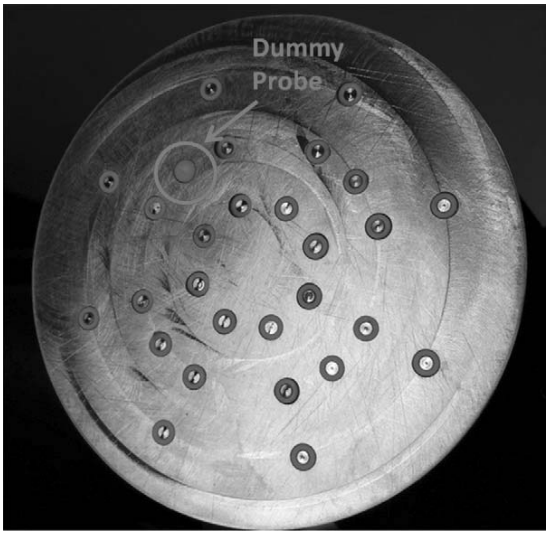

Figure 2. The CFPA as seen from the front after assembly. The 28 probes are divided into 4 quadrants of 4 probes, with the dummy probe as the middle probe in one of the quadrants. Probes with ceramic sheath can be seen.

two adjacent probe heads of different radial positions but identical azumithal positon, a measurement of the radial current was obtained. By connecting two adjacent probe heads of different azumithal position, but identical radial position, a measurement of the azumithal current was obtained. Finally, by measuring the current through a resistor between the probe head and ground, a measurement of the axial current was obtained. Since TELS is a pulsed device, it was thought that displacement currents might comprise a significant portion of the measured current even though the signal cables were properly shielded. For this reason, a dummy probe, identical to the others except that the face is covered in ceramic was installed in place of one live probe. Displacement currents as measured by the dummy probe were $<1\%$ of the currents measured by the CFPA, and are subtracted from the currents presented

Table 1. Compilation of the results of the flush probe experiments showing the maximum and typical currents.

Coax gun voltage (kV)	5.5	5.5	6	6
Chamber static fill (mTorr)	160	160	160	160
Theta voltage (kV)	0	16	0	16
Typical radial current (kA m^{-2})	109^{+60}_{-30}	84^{+49}_{-15}	150^{+56}_{-57}	110^{+39}_{-29}
Max radial current (kA m^{-2})	407	236	544	158
Typical azumithal current (kA m^{-2})	84^{+45}_{-20}	72^{+37}_{-15}	100^{+43}_{-41}	80^{+36}_{-24}
Max azumithal current (kA m^{-2})	371	142	387	189
Surface velocity, cross correlation (km s^{-1})	4.95 ± 1.18	3.6 ± 3	6 ± 0.75	3.5 ± 3
Surface velocity, bulk axial ToA (km s^{-1})	4	12.2	5.6	15.9
Maximum stable dimension (mm) avg.	12	8.3	7.5	5.4
Maximum stable dimension (mm) min.	5.7	6.1	3.7	4.9

Note: A maximum on the surface velocity is also shown in table along with the maximum stable liquid lithium surface dimension as predicted by linear stability theory.

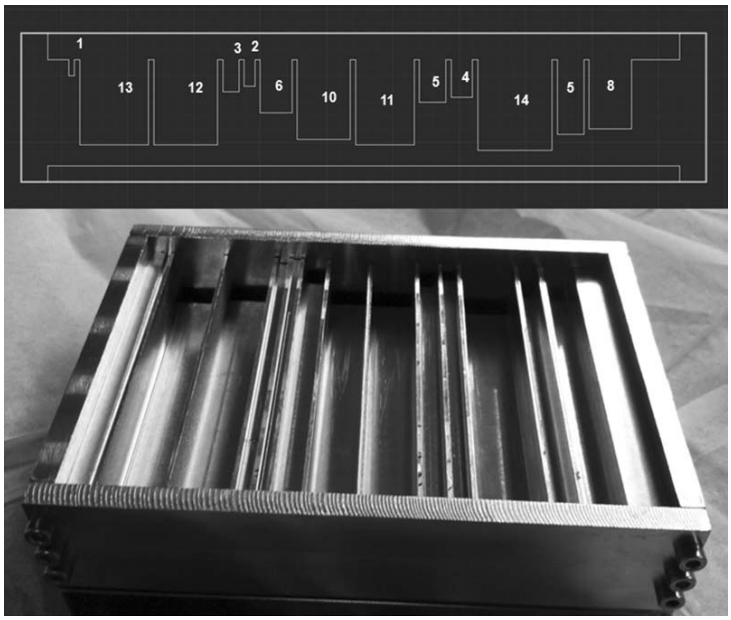

Figure 3. (Above) Schematic of the side view of the special LiMIT channels. Trench width is displayed in millimeters. (Below) Photograph of the LiMIT trenches as assembled. Trenches were subsequently installed into the TELS chamber and filled.

here. Plasma velocity, important for stability to KH instabilities, was characterized both by analysis of the cross correlation between different current traces, similar to a method used for the characterization of resistive drift waves in the VINETA device at IPP Greifswald [13] and also by a comparison of the time of arrival of axial currents to the various probe heads.

The results of these measurements were then utilized in the linear stability analysis performed earlier to determine the maximum stable lithium surface dimension in each of the experimental conditions. Table 1 shows a summary of the current, magnetic field and velocity measurements as well as the result of the analysis for the maximum stable lithium dimension.

4. Lithium stability experiments

To test the predictions of the linear stability analysis, a special version of the LiMIT device was constructed. A series of LiMIT trenches were machined with different trench widths ranging from 1 to 14 mm in width. A picture and side-view schematic of these trenches can be seen in figure 3. These trenches were then placed into the TELS chamber and fired upon with the same shot parameters investigated earlier. A fast frame camera observed the shots to record instances of ejection.

The initial round of tests with the variable width trenches was conducted on only partially filled and unwetted trenches. For these tests, there was a drop of lithium in the 10 and 11 mm trenches as well as a pool at the bottom of the trenches. The lithium did not wet the trenches in this case.

Ejected particles from each of the unwetted shots were ray-traced back to only the 10 and 11 mm trenches as well as the lithium pool at the base of the trenches. These ejected particles are assumed to be from the unwetted droplets in each of the 10 and 11 mm trenches (as well as the unwetted pool of lithium). Ejection was seen in the cases of the 5.5 and 6 kV coaxial gun shots with and without the theta pinch.

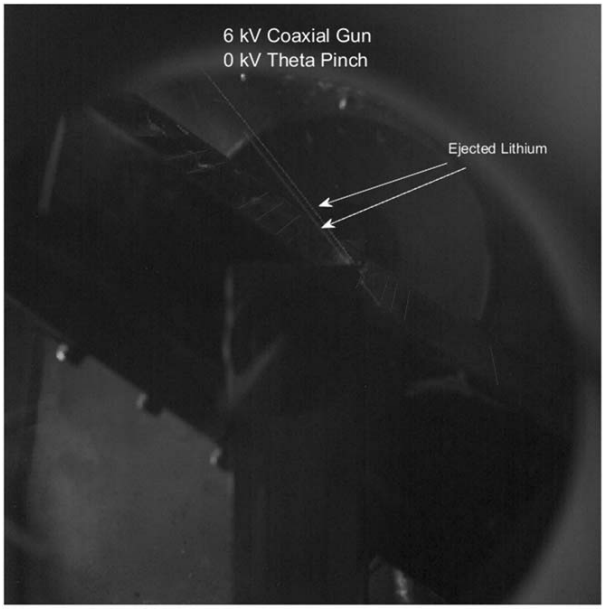

Figure 4. Fast frame camera frame after plasma impact. Multiple ejections are observed, this time above the 26 mm boundary. However, the lithium pool that overflowed the 26 mm trench is also contiguous across the 2, 3, and 6 mm trenches and has a boundary at the edge of the 22 mm trench above it. Ejection observed from 2 of the boundaries of this pool (one from the upper boundary, one from the near wall) during this frame.

Subsequent tests completely filled and wetted the lithium channels. The temperature of the trenches during injection was raised in excess of 400 °C in order to ensure lithium wetting of the trenches. During filling, evaporation of the lithium was observed, but inspection of the trenches both after filling and after removal from the chamber showed clear evidence of fully filled lithium trenches that were well wetted. These filled trenches were then viewed by the fast frame camera, and inspected for ejection of lithium. During these shots however, none of the trenches showed ejection under any of the shot conditions investigated.

It was expected that ejection would occur at least in the 13 and 14 mm trenches during each of the shot conditions. The lack of ejection from the 1–14 mm trenches demonstrates that the initial RT–KH stability boundary underestimates the maximum stable trench dimension. Consequently, a series of larger trench dimensions were sought to properly capture the location of the experimental stability boundary. The trench structure was modified by removing the 1 mm wall between the 12 and 13 mm trenches as well as the wall between the 10 and 11 mm trenches in order to make a 22 mm and 26 mm trench.

A still frames captured from the the 6 kV coaxial, 0 kV theta shot is shown in figure 4. For each exposure case, significant ejection from the lithium pool, which included the 26 mm trench, at the base of the TELS trenches was observed during exposure to the coaxial gun plasma shots with and without the theta pinch. However, no ejection was observed from the 22 mm trench, indicating that the stability boundary is greater than 22 mm, and lies in the neighborhood of 26 mm for each of the shot conditions investigated. Ejection of lithium was

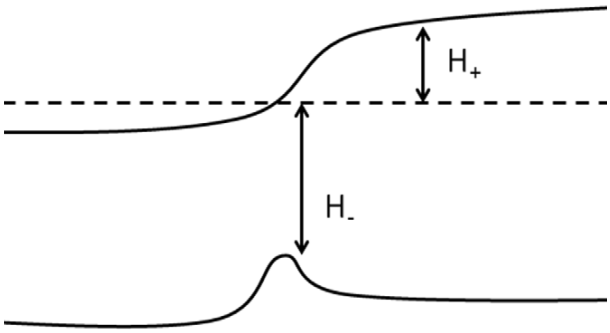

Figure 5. Diagram of height of liquid surface in derivation of modified shallow water equations. H_+ is the height of the water above the unperturbed line. H_- is the depth of the water below the unperturbed line. H, the height of the total water column is then the sum of H_- and H_+.

strongest from the 6 kV coaxial gun shots. However, lithium ejection was observed under each of the shot conditions. Ejection was also observed to be greatest from the edges and corners of the trenches. Only under the 6 kV coaxial gun shots was lithium observed to eject from the trench center. It is clear from these tests however, that the experimental stability boundary of lithium deviates from the analytic stability boundary derived previously.

Additional analysis was performed to further confirm that the experimentally observed stability boundary is different from the analytic stability boundary. First, a sensitivity analysis was performed with regard to the physical constants used in the analytic stability analysis. Surface tension, for example, may be altered by the chemical composition of the lithium surface (i.e. the presence of lithium compounds). Another example may be given by the fact that the density of liquid lithium is temperature dependent. Since the current and magnetic field were directly measured, any discrepancy between the theory and the experiment must be accounted for by a difference in surface tension or density if the previous stability boundary is still considered to be correct. Recent results [14] have shown the dependence of the surface tension of common lithium compounds on temperature. These tests show that the common lithium compounds (oxide, hydroxide, nitride) that would form in a fusion reactor serve to decrease the value (0.3–0.35 N m^{-1}) of the surface tension of lithium with respect to the surface tension of a clean lithium surface (0.4 N m^{-1}) [15]. Therefore, the presence of lithium compounds polluting the lithium surface would cause a decrease in the maximum stable dimension predicted by the analytic stability boundary rather than the observed increase. Similarly, the difference in density of lithium at 300 °C (504 kg m^{-3}) and as high as 500 °C (486 kg m^{-3}) [15] is not sufficient to explain the departure.

It has also been suggested that the discrepancy may be due to the strong dependence of the analytic stability boundary on the interpretation of the critical wavenumber. Linear stability theory identifies a critical wavenumber rather than a critical dimension. Here, the critical wavenumber was interpreted to be the smallest wavenumber for which one half-wavelength fit within the trench width. If the interpretation is changed such that

the critical wavenumber correlates to a full wavelength fitting within one trench or 1.5 wavelengths fitting inside the trench, the results are still not consistent. For example, if the critical wavelength is assumed to equate to a full wavelength fitting inside the trench width. The stable dimension predicted for the 5.5 kV coaxial gun shot without a theta pinch is 23 mm, which matches the experiment. However, the stable dimension predicted for the 6 kV coaxial gun shot with a theta pinch is 7.5 mm, which is very different from the experimental observation. No interpretation of the critical wavelength is able to satisfy all of the experimental results, therefore, a new theory is sought.

5. Shallow water theory

To explain the observed discrepancies between the Rayleigh–Taylor/Kelvin–Helmholtz theory presented earlier and the experimental results presented in the previous section as well as figure 4, the authors reexamine the experimental results and compare to a new analysis. In most cases, the ejection occurred from an edge of one of the channels. Much more rarely, did the ejection of droplets occur from the center of the trenches. Droplet ejection in this case is attributed to splashing of waves induced by Rayleigh–Taylor (RT) and Kelvin–Helmholtz (KH) drivers rather than a more conventional RT–KH driven disruption. Shallow water theory is used to model the propagation of waves generated on the surface of the lithium. Shallow water theory is a simplification of the Navier–Stokes equations in the limit that the wavelengths of the perturbations on the surface of the fluid are longer than the depth of the fluid [16]. It is used in oceanography for the modelling of tsunamis and additionally can be applied in the modelling of waves in a tub [17]. The derivation of the following shallow water equations follows a derivation similar to [16] with the addition of surface tension terms. Beginning with the Navier Stokes equations with the assumption of incompressible flow, and employing a dyadic form for the advective terms rather than the more common $v \cdot \nabla v$ form:

$$\nabla \cdot v = 0 \tag{2}$$

$$\frac{\mathrm{d}v}{\mathrm{d}t} + \nabla \cdot (vv) = -\frac{\nabla P}{\rho} + g + \frac{1}{\rho}\nabla \cdot T. \tag{3}$$

Let us model the water height with two variables, H_- and H_+ demonstrated in figure 5. The total height of the water, H, is then the sum of H_- and H_+. The boundary conditions are then defined as no flow normal to the boundary on the top and bottom boundaries:

$$\left(\frac{\mathrm{d}H}{\mathrm{d}t} + v \cdot \nabla H = v_z\right)\Big|_{z=H_+,\, z=-H_-}. \tag{4}$$

Due to the low viscosity of lithium, drag on the bottom surface of the lithium is neglected, because even if a full slip condition is imposed, the low viscosity of lithium ensures a thin boundary layer, which may be neglected:

$$\hat{n}_- \cdot T = 0 = \tau_{xx}\frac{\mathrm{d}H_-}{\mathrm{d}x} + \tau_{xy}\frac{\mathrm{d}H_-}{\mathrm{d}y} + \tau_{xz} \tag{5}$$

Where $\hat{n}$ is the surface normal and τ is the surface shear. The boundary stress condition on the top surface is given by surface tension:

$$\hat{n}_+ \cdot T = \sigma\hat{n}(\nabla \cdot \hat{n}) - \nabla\sigma = \tau_{xx}\frac{\mathrm{d}H_+}{\mathrm{d}x} + \tau_{xy}\frac{\mathrm{d}H_+}{\mathrm{d}y} + \tau_{xz} \tag{6}$$

From which we neglect surface tension gradients, which holds in the case of the clean and nearly isothermal lithium surface employed in the experiments herein. Shallow water theory employs depth averaged profiles for the x and y velocities, a consequence of the assumption that the perturbation wavelengths are longer than the depth. As a result, the shallow water continuity equation is a depth average of the Navier–Stokes continuity equation:

$$\int_{-H_-}^{H_+}\left(\frac{\mathrm{d}v_x}{\mathrm{d}x} + \frac{\mathrm{d}v_y}{\mathrm{d}y} + \frac{\mathrm{d}v_z}{\mathrm{d}z} = 0\right)\mathrm{d}z \tag{7}$$

$$\int_{-H_-}^{H_+}\left(\frac{\mathrm{d}v_x}{\mathrm{d}x} + \frac{\mathrm{d}v_y}{\mathrm{d}y}\right)\mathrm{d}z + v_z|_{H_+} - v_z|_{H_-} = 0. \tag{8}$$

Employing the Leibniz integral rule to the first two terms yields:

$$\int_{-H_-}^{H_+}\left(\frac{\mathrm{d}v_x}{\mathrm{d}x}\right)\mathrm{d}z = \frac{\mathrm{d}}{\mathrm{d}x}\int_{-H_-}^{H_+} v_x\mathrm{d}z - v_x|_{H_+}\frac{\mathrm{d}H_+}{\mathrm{d}x} - v_x|_{H_-}\frac{\mathrm{d}H_-}{\mathrm{d}x}. \tag{9}$$

Let the integral of velocity over height be equal to a height averaged velocity times the height:

$$\int_{-H_-}^{H_+} v_x\mathrm{d}z = H\,\overline{v_x}. \tag{10}$$

By employing (10) and the two no normal flow boundary conditions (6), the shallow water equation for continuity, (9), becomes:

$$\frac{\mathrm{d}H}{\mathrm{d}t} + \frac{\mathrm{d}}{\mathrm{d}x}(H\,\overline{v_x}) + \frac{\mathrm{d}}{\mathrm{d}y}\left(H\,\overline{v_y}\right) = 0. \tag{11}$$

By similar analysis and once again employing the boundary conditions in (6), the left hand side of the x-momentum equation (5) reduces to:

$$\frac{\mathrm{d}}{\mathrm{d}t}(H\,\overline{v_x}) + \frac{\mathrm{d}}{\mathrm{d}x}(H\,\overline{v_x}^2) + \frac{\mathrm{d}}{\mathrm{d}y}(H(\overline{v_x})(\overline{v_y})). \tag{12}$$

Since the pressure internal to the lithium is assumed to be due to hydrostatic equilibrium, addressing the right hand side of the x-momentum equation begins with the following integration:

$$\int_{-H_-}^{H_+}\left(-g\frac{\mathrm{d}H_+}{\mathrm{d}x} + \frac{\mathrm{d}}{\mathrm{d}x}(\tau_{xx}) + \frac{\mathrm{d}}{\mathrm{d}y}(\tau_{xy}) + \frac{\mathrm{d}}{\mathrm{d}z}(\tau_{xz})\right)\mathrm{d}z. \tag{13}$$

Once again employing the Leibniz rule, as in (11), as well as applying the boundary condition in (7) and (8), the right hand side of the x-momentum equation collapses to:

$$-gH\frac{\mathrm{d}H_+}{\mathrm{d}x} + \frac{\sigma}{\rho}\hat{n}(\nabla \cdot \hat{n}). \tag{14}$$

Under the assumption that there are no body forces other than gravity acting on the lithium. Since the TELS plasma is a

pulsed device and the ejection occurs on a much longer time scale than that of the plasma, this is a justified assumption for the case of this transient impinging on the free lithium surface after the impingement of the transient. Constraining the solution to a constant H_{-}, i.e. the depth of the fluid floor is a constant, again true for the lithium channels considered here, and rearranging. The x-momentum equation in its entirety can then be written as:

$$\frac{\mathrm{d}}{\mathrm{d}t}(H\overline{v_x})+\frac{\mathrm{d}}{\mathrm{d}x}\left(H\overline{v_x}^2+\frac{1}{2}gH^2\right)+\frac{\mathrm{d}}{\mathrm{d}y}(H(\overline{v_x})(\overline{v_y})) = \left(\frac{\sigma}{\rho}\hat{n}(\nabla\cdot\hat{n})\right)\cdot\hat{x}. \tag{15}$$

Again, invoking the argument of long wavelength as compared to depth, the surface normal may be approximated as:

$$\hat{n}=-\frac{\mathrm{d}H}{\mathrm{d}x}\hat{x}-\frac{\mathrm{d}H}{\mathrm{d}y}\hat{y}+\hat{z}. \tag{16}$$

Evaluating the full surface tension term:

$$\frac{\sigma}{\rho}n(\nabla\cdot n)=\frac{\sigma}{\rho}\frac{\mathrm{d}H}{\mathrm{d}x}\left(\frac{\mathrm{d}^2H}{\mathrm{d}x^2}+\frac{\mathrm{d}^2H}{\mathrm{d}y^2}\right)\hat{x}+\frac{\sigma}{\rho}\frac{\mathrm{d}H}{\mathrm{d}y}\left(\frac{\mathrm{d}^2H}{\mathrm{d}x^2}+\frac{\mathrm{d}^2H}{\mathrm{d}y^2}\right)\hat{y}. \tag{17}$$

The combination of (11), (15), and equivalent equation in y for (15) compose the shallow water equations modified here to include surface tension.

The shallow water equations are typically solved numerically [18]. uses a Lax–Wendroff algorithm to numerically solve the shallow water equations. The Lax–Wendroff solver from [18] was modified to include the surface tension terms detailed in equation (17). In this model, the height of a pool of liquid is perturbed with a Gaussian, simulating addition of momentum to the pool. The waves generated by the perturbation are then allowed to propagate with reflecting boundary conditions on each edge of the computational domain. A series of images showing the initial disturbance to the liquid height as well as the subsequent propagation can be seen in figure 6. As can be seen from figure 6, the waves bounce off the side walls, and interfere with the various reflections in the center of the lithium pool. Since there is no dissipation in the shallow water equations derived here, and since the Lax–Wendroff solver is explicit in its time-stepping, this model is only valid for small times. The dissipation of the capillary-gravity waves induced on the surface of the lithium is given in detail by [19], showing strong damping in both the short wavelength and long (but only in finite depth conditions) wavelength regimes. Here, only the quasi-inviscid root is considered:

$$\mathrm{Im}(\omega)\sim 2\nu k^2 \tag{18}$$

where ν is the kinematic viscosity. Since the dissipation time (~0.3 s) for the observed capillary-gravity waves is longer than the wave bounce time (<0.01 s), the Lax–Wendroff model is taken to be accurate in time through the first set of reflections from the walls of the computational domain. It is further hypothesized that ejection of droplets occurs when the curvature of the surface is great enough that it is energetically favorable for the lithium pool to eject a droplet. It can be seen from the model that the areas of greatest curvature are observed along the boundaries of the lithium pool, consistent with the observation that the majority of the lithium ejection observed in the experiments comes from the edges of the lithium trenches. However, under strong enough displacements of the lithium, constructive interference of waves reflecting off of the sides of the channel results in an area of large curvature, again consistent with the observation that certain plasma bombardments, in this case, the plasma bombardments with the largest currents, can still eject lithium from the center of the channels.

To determine the critical curvature for ejection of lithium, Plateau–Rayleigh breakup of a liquid stream into droplets is invoked. In Plateau–Rayleigh theory, growing (unstable) oscillations on the sides of a liquid column cause pinch off of the liquid column into droplets. A full discussion of Plateau–Rayleigh breakup of liquid columns can be found in [20], and its application to liquid lithium has predicted the breakup of a lithium jet into droplets previously [21].

Considering a column of liquid with height H, and radius R and allowing perturbations with half-wavelength equal to the height of the liquid column, the stability criterion may be written as:

$$\pi<\frac{H}{R}. \tag{19}$$

If this criterion is satisfied, the column may be considered unstable to Plateau–Rayleigh instabilities. Since the lithium surface does not naturally form cylinders, we instead take the height as the height of the liquid, and R as the local radius of curvature of the surface, R_c:

$$0<\frac{H}{\pi R_\mathrm{c}}-1. \tag{20}$$

To determine if a lithium trench is unstable to lithium ejection, the Lax–Wendroff model is employed while monitoring the quantity in equation (20). First, a perturbation to the surface is introduced. The size of the perturbation is set such that the momentum induced by the perturbation is equal to that of the momentum deposited by the Rayleigh–Taylor and Kelvin–Helmholtz drivers:

$$\int_{t_o}^{t_\mathrm{final}}\left(\iiint(J\times B)\mathrm{d}V\right)\mathrm{d}t + \int_{t_o}^{t_\mathrm{final}}\left(\iint\left(\frac{\rho_\mathrm{pl}\rho_\mathrm{Li}}{\rho_\mathrm{pl}+\rho_\mathrm{Li}}(v_\mathrm{pl}-v_\mathrm{Li})^2\right)\mathrm{d}A\right)\mathrm{d}t = \sqrt{2*\iiint_\mathrm{perturbation}\rho\mathrm{d}V\iiint_\mathrm{perturbation}\rho g\mathrm{d}V} + \int_{t_o}^{t_\mathrm{final}}\left(\iint\left(\frac{\sigma}{R_\mathrm{c}}\right)\mathrm{d}A\right)\mathrm{d}t. \tag{21}$$

The perturbation is then allowed to propagate while the quantity in equation (20) is tracked for all locations on the surface as a function of time after the first reflection off of the trench walls, monitoring for locations where the quantity exceeds 0 (i.e. unstable locations). The results of the stability analysis can be seen in figure 7. To generate these stability contours, a

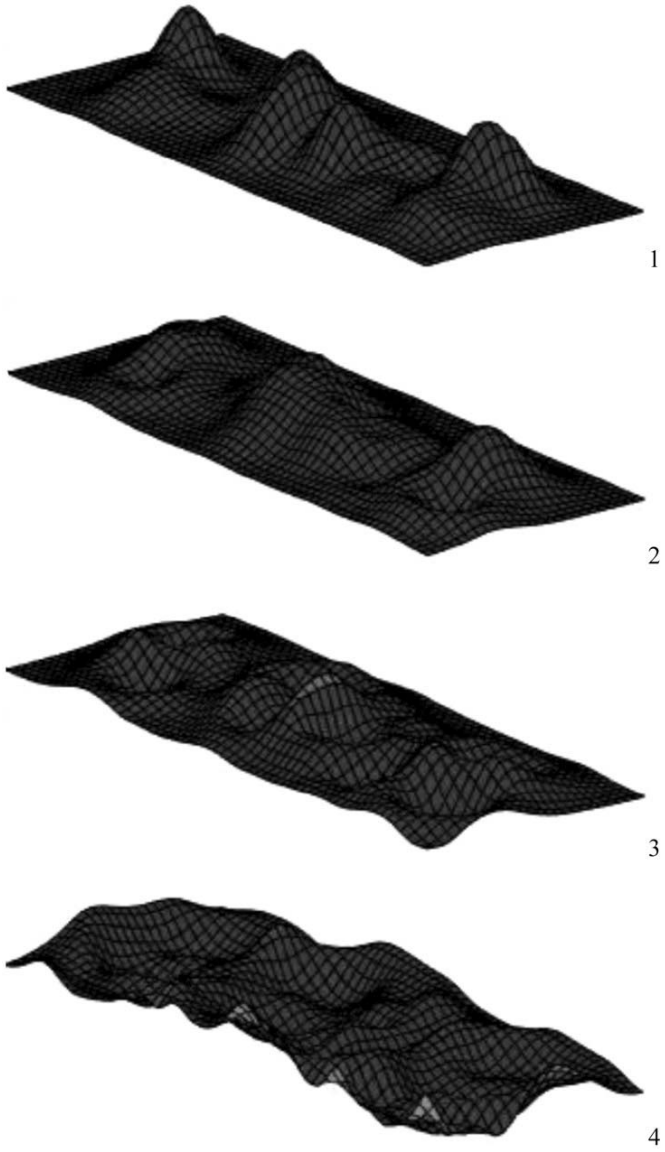

Figure 6. Unstable propagation of waves on the lithium surface as calculated by the Lax–Wendroff model. Unstable areas are marked in red, stable areas are dark cyan. Initial disturbances driven by Gaussian perturbations to the surface. Reflections of the waves can be seen off of the side walls and interference of the waves can be observed in the center of the trenches.

series of simulations were run with the Lax–Wendroff solver for a variety of plasma impulses and trench dimensions. Cases exhibiting no ejection, edge ejection, and center and edge ejection were marked as such and contours were then plotted. Like the stability curves from the analytic stability criterion presented previously, the stability of the liquid lithium surface is dependent on trench dimension, however, the critically stable trench dimension is larger in this analysis. In both figures 7(*A*) and (*B*), the *x*-axis is given as the normalized plasma impulse for a 120 kA m^{-2} Rayleigh–Taylor driver in a 0.22 T magnetic field with no Kelvin–Helmholtz driver. The conversion is given by equation (22):

$$x = \frac{J(\text{kA m}^{-2})B(\text{T})}{120 * 0.22} + \frac{0.02(v(\text{km s}^{-1}))^2}{w\ (\text{mm})} \tag{22}$$

where J is the current density in kA m^{-2}, B is the magnetic field in T, v is the plasma velocity in km s^{-1}, and w is the trench width in mm. The approximate stability boundary, shown with a dashed line in figure 7, was a fit to data and may be then given heuristically by:

$$w\ (\text{mm}) = \frac{15}{x^{0.75}} + \frac{10}{x^{0.5}} \tag{23}$$

where w, the maximum stable width in millimeters, is given as an inverse power function of the normalized plasma impulse. The stability boundary shown in figure 7 is significantly larger than that predicted by the linear stability theory laid out before. From these curves it can be seen that the 5.5 kV coaxial shots, with and without the theta pinch, are more stable than the 6 kV coaxial shots, as is also predicted by linear stability theory,

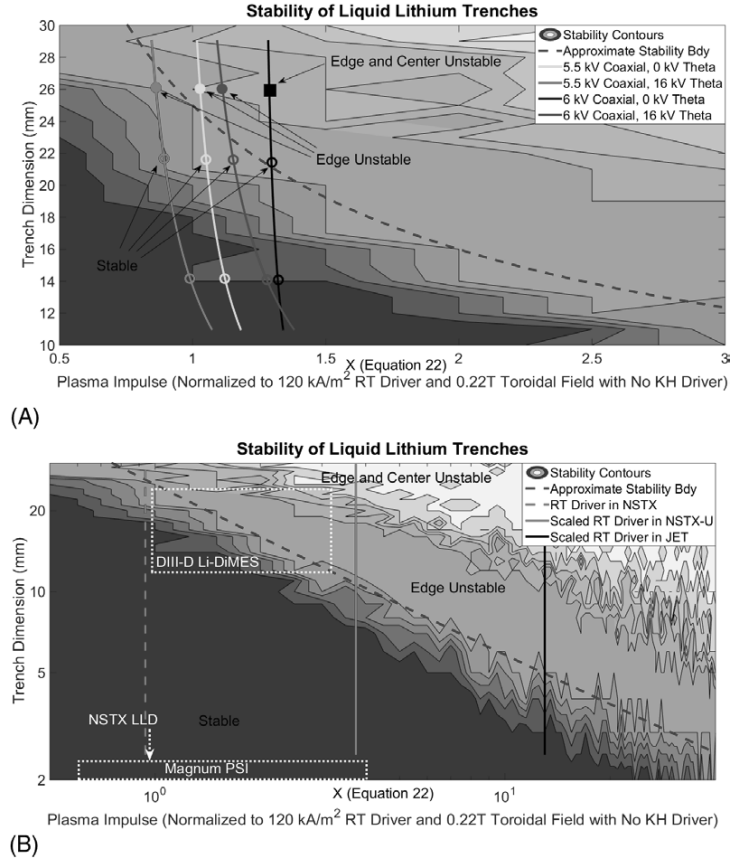

Figure 7. (*A*) Stability contours as obtained from the modified shallow water equation model. Dark blue regions are stable to plasma impingement. Turquoise regions are unstable to edge ejections. Yellow regions are unstable to both edge and center ejections of lithium. Contours are overlaid with curves of the plasma impulse delivered by TELS as measured experimentally by the CFPA. Plasma impulse delivered is in units of momentum normalized to the momentum input from a 120 kA m^{-2} current in a 0.22 T magnetic field and no plasma velocity tangential to the surface. The approximate stability boundary from equation (23) is drawn as a guide. Experimental results are overlaid, with open marks for stable experimental points, closed circles for edge unstable shots, and closed squares for edge and center unstable shots. (*B*) Stability contours of lithium where dark blue regions are stable to plasma impingement. Turquoise regions are unstable to edge ejections. Yellow regions are unstable to both edge and center ejections of lithium. Contours are overlaid with curves of the plasma impulses delivered by NSTX and an impulse delivered by JET scaled from the NSTX currents. Plasma impulse delivered is in units of momentum normalized to the momentum input from a 120 kA m^{-2} current with an 0.22 T toroidal field and no plasma velocity tangential to the surface. Plasma impulse is calculated from equation (21) with $\jmath$ given by the PFC current as in [8] and (*B*) given by the main toroidal field. For tokamaks where the PFC current has not been measured, PFC current is assumed to scale linearly with plasma current.

however, the stability boundary predicted by modified shallow water theory is much more accurate. The stability boundary predicted for the shots performed in TELS is approximately 22–28 mm as observed in experiments where the 22 mm trench did not eject, but the 26 mm trench did eject. Modified shallow water theory also correctly anticipates ejection from the center of the large lithium pool during the 6 kV coaxial shots with no theta pinch only. The range of plasma impulse in the experiments detailed here, however, is still small. As such, we turn to the remaining data that is available and compare experiment to theory. Figure 7(*B*) replots the stability boundary from modified shallow water theory with the stability regions from the LiMIT experiments performed at Magnum PSI and the Li-DIMES experiment. In the Magnum PSI experiments, droplets were not observed to eject from the LiMIT channels. This is commensurate with the stability contours that are presented here which predict stability for those experiments. The Li-DIMES experiment meanwhile falls squarely across the stability boundary. This again is consistent with experimentation which showed ejection in some shots, but not others. The NSTX LLD experiments fall well within the stability region in figure 7, with a critical dimension smaller than what is shown on the impulse line for NSTX, consistent with the stability observed experimentally. To extend the theory to a variety of machines, proper measurement of the currents flowing in the PFCs is necessary. In the interim, several vertical lines are shown in figure 7 representing the expected plasma impulse from several major machines under the assumption that PFC currents scale linearly plasma current. Also, while exhaustive proof that the modified shallow water theory stability boundary will correctly predict stability of a PFC lithium surface under all circumstances is not yet presented, experimental results both obtained here and elsewhere are consistent with the stability boundary derived in this paper. More experiments are needed at larger plasma impulses to properly map the stability boundary and confirm the validity of this lithium stability theory.

6. Conclusions

The stability of liquid metal plasma facing components was analyzed using the TELS device at the University of Illinois. A flush probe array was used to measure axial, azumithal, and radial currents under four different TELS shot conditions. The flush probe was also used to characterize a maximum on the surface velocity of the plasma across the lithium surface. These measurements were then implemented in a linear stability analysis to determine the maximum stable lithium surface dimension for a given set of experimental conditions. A set of special lithium LiMIT trenches were prepared and installed into the TELS device and fired upon. Ejections were tracked with a fast frame camera and compared to the linear stability analysis. A variety of trench structures were exposed within the TELS chamber to the coaxial gun plasma shots with and without the theta pinch. It was found that ejection depended on a multiple of variables, some not immediately obvious. The first of these influences to be observed was wetting of the lithium trenches. Under unwet conditions, the lithium ejected droplets readily under plasma exposure. Variable width trenches inserted into the chamber to investigate the dependence of the stability boundary on trench dimension during wetted conditions showed results that were considered anomalous at first. However, after repeated exposures to similar conditions, it was seen that the linear stability theory detailed previously was incorrect in its description of the physics undergone by lithium under transient plasma exposure. Trenches between 1 and 14 mm in width did not eject under multiple tests, even when the trenches were reversed to investigate if the effect was purely due to spatial variation of the plasma on target. Subsequent exposure of much larger trenches showed strong evidence of lithium ejection under all tested plasma exposure conditions. Strongest ejection was observed during the 6 kV coaxial gun 0 kV theta shots, which is commensurate with the shot conditions under which the largest radial/azumithal currents were delivered to the CFPA, suggesting that the current driven instabilities dominate over the plasma velocity driven instabilities for the trench dimensions investigated in this work. Furthermore, a new stability theory was derived based on shallow water theory with modifications made to include surface tension forces. A Plateau–Rayleigh like condition was enforced to determine whether or not a given trench would eject lithium. Commensurate with the experiments, this theory predicted that edge ejection (wave splashing against the wall) would dominate over ejection from the center of the trenches (constructive wave interference). Also commensurate with the experiments, this theory predicted a stability boundary between 22 and 28 mm for all of the shot conditions investigated. This was confirmed in experiments where the 22 mm trench in all scenarios did not eject lithium, but the 26 mm trench did in all cases. Finally, the conditions for lithium ejection were predicted to be met in the center of the 26 mm trench only in the case of the 6 kV coaxial gun and 0 kV theta shots, which was also observed experimentally.

References

[1] Whyte D.G., Evans T.E., Wong C.P.C., West W.P., Bastasz R., Allain J.P. and Brooks J.N. 2004 Experimental observations of lithium as a plasma-facing surface in the D-IIID tokamak divertor *Fusion Eng. Des.* **72** 133–47

[2] Bazylev B., Landman I., Loarte A., Klimov N.S., Podkovyrov V.L. and Safranov V.M. 2009 Experiments and modelling of droplet emission from tungsten under transient heat loads *Phys. Scr.* **T138** 014061

[3] Lipschultz B., Coenen J.W., Barnard H.S., Howard N.T., Reinke M.L., Whyte D.G. and Wright G.M. 2012 Divertor tungsten tile melting and its effect on core plasma performance *Nucl. Fusion* **52** 123002

[4] Majeski R. *et al* 2004 Testing of liquid lithium limiters in CDX-U *Fusion Eng. Des.* **72** 121–32

[5] Ruzic D.N., Xu W., Andruczyk D. and Jaworski M.A. 2011 Lithium-metal infused trenches (LiMIT) for heat removal in fusion devices *Nucl. Fusion* **51** 102002

[6] Ren J., Hu J.S., Zuo G.Z., Sun Z., Li J.G., Ruzic D.N. and Zakharov L.E. 2014 First results of flowing liquid lithium limiter in HT-7 *Phys. Scr.* **T159** 014033

[7] Fiflis P., Morgan T.W., Brons S., Van Eden G.G., Van den Berg M.A., Xu W., Curreli D. and Ruzic D.N. 2015 Performance of the lithium metal infused trenches in the magnum PSI linear plasma simulator *Nucl. Fusion* **55** 113004

[8] Jaworski M.A. *et al* 2013 Liquid lithium divertor characteristics and plasma-material interactions in NSTX high-performance plasmas *Nucl. Fusion* **53** 083032

[9] Eich T., Kallenbach A., Pitts R.A., Jachmich S., Fuchs J.C., Herrmann A., Neuhauser J. and ASDEX Upgrade Team, and JET-EFDA Contributors 2007 Divertor power deposition and target current asymmetries during type-1 ELMs in ASDEX upgrade and JET *J. Nucl. Mater.* **365** 989–93

[10] Christenson M. 2015 Characterization of ion properties in a linear pulsed plasma-material interaction test stand *Master's Thesis* UIUC

[11] Jung S. 2014 Development of high energy pulsed plasma simulator for plasma-lithium trench experiment *Doctoral Thesis* UIUC

[12] Kallman J., Jaworski M.A., Kaita R., Kugel H. and Gray T.K. 2010 High density Langmuir probe array for NSTX scrape-off layer measurements under lithiated divertor conditions *Rev. Sci. Instrum.* **81** 10E117

[13] Schroder C. 2003 Experimental investigations on drift waves in linear magnetized plasmas *Doctoral Thesis* Ernst-Moritz-Arndt-Universitat, Greifswald

[14] Krat S.A., Popkov A.S., Gasparyan Y.M., Pisarev A.A., Fiflis P., Szott M., Christenson M., Kalathiparambil K. and Ruzic D.N. 2016 Wetting properties of liquid lithium on lithium compounds *Fusion Eng. Des.* at press

[15] Zinkle S.J. 1998 Summary of physical properties of lithium, Pb-17Li, and $(LiF)_nBeF_2$ coolants *APEX Meeting (Los Angeles, 2–4 November 1998)* vol 4 (UCLA)

[16] Dawson C. and Mirabato M. 2008 The shallow water equations (online)

[17] Vallis G. 2006 *Atmospheric and Oceanic Fluid Dynamics* (Cambridge: Cambridge University Press)

[18] Moler C. Experiments with MATLAB (online)

[19] LeBlond P.H. and Mainardi F. 1987 The viscous damping of capillary-gravity waves *Acta Mech.* **68** 203–22

[20] de Gennes P.G., Brochard-Wyart F. and Quere D. 2004 *Capillary and Wetting Phenomena* (Berlin: Springer)

[21] Fiflis P., Andruczyk D., Roquemore L., McGuire M., Curreli D. and Ruzic D.N. 2013 Lithium pellet production (LiPP): a device for the production of small spheres of lithium *Rev. Sci. Instrum.* **84** 063506